Effect of Warm Temperatures on Externally Bonded FRP Strengthening

The Effect of Warm Temperatures on Externally Bonded FRP Strengthening

T.J. Stratford [1] and L.A. Bisby [2]

1 Corresponding author.
Senior Lecturer, Joint Research Institute for Civil and Environmental Engineering, School of Engineering, The University of Edinburgh, The King's Buildings, Edinburgh, EH9 3JL, Scotland, UK.
E-mail: Tim.Stratford@ed.ac.uk

2 Reader, BRE Centre for Fire Safety Engineering, School of Engineering, The University of Edinburgh, The King's Buildings, Edinburgh, EH9 3JL, Scotland, UK.
E-mail: Luke.Bisby@ed.ac.uk

ABSTRACT

Fiber-reinforced polymer (FRP) plate strengthening relies critically upon the adhesive that is used to bond it to the existing structure. A typical two-part ambient cure epoxy adhesive for structural strengthening has a glass transition temperature that is around 40ºC to 70ºC, but the stiffness and strength of the adhesive typically decrease at temperatures somewhat below this characteristic temperature. This paper investigates the implications of the changes in adhesive properties at warm temperatures (< 100°C) for FRP strengthened beams, through short-term experimental and analytical work. Tests were conducted on FRP-strengthened steel beams subjected to sustained load and increasing temperature; the results, however, are also relevant to strengthened concrete beams. Digital image correlation was used to measure the slip between the strengthening plate and beam, and hence to observe the behavior of the adhesive joint. A bond analysis was also developed to predict the slip across the adhesive joint at elevated temperature, based upon the glass transition characteristics of the adhesive measured using dynamic mechanical analysis. The analysis allows the response of the strengthened beams to warm temperatures to be examined in further detail. Both the experimental and analytical results show that substantial slip can occur between the plate and beam at temperatures over 40ºC. As the temperature increases and the adhesive softens, a greater length of adhesive joint is required to transfer load from the plate to the beam, resulting in an increase in slip that eventually causes debonding of the plate from the beam.

KEYWORDS

Adhesive, Bond, Temperature, Fiber-reinforced polymer, Strengthening, Steel, Experiment, Analysis

INTRODUCTION

The popularity of externally-bonded fiber-reinforced polymer (FRP) strengthening is largely due to the ease with which it can be applied to concrete (ACI 2008; Concrete Society 2004) and metallic (CIRIA 2004; CNR 2007; Schnerch 2007) structures. This ease of installation usually relies upon ambient-cure epoxy bonding adhesives, allowing strengthening without the need for elevated temperature cure. These ambient-cure epoxies, however, have glass transition temperatures (T_g) of between 40 and 70°C (ACI 2008; Concrete Society 2004). The glass transition describes 'softening' of the adhesive as it changes from a glassy to a rubbery state, but this does not occur at a single temperature, and the stiffness and strength of the adhesive may decrease considerably before T_g has been reached.

Research into the elevated temperature performance of FRP strengthening has concentrated upon the 'hot' temperatures that occur during fire (Kodur *et al.* 2007). This paper, however, investigates the performance of bonded FRP strengthening at 'warm' temperatures (below 100ºC), which are comparable to the glass transition temperature of the adhesive. These temperatures are possible during the normal service of a strengthened structure; for example, comparable temperatures are considered during the design of steel highways bridges in the UK (Highways Agency 2001).

The need for research into elevated temperature response was highlighted by Porter and Harries (2007) in their review of FRP research requirements, but there has so far been only a limited amount of research on 'warm' temperatures upon FRP-strengthening. Klamer *et al.* (2008) load tested FRP-strengthened concrete beams at 20, 50 and 70ºC and showed that whilst the performance of the FRP strengthening was not adversely affected at 50ºC, their load capacity was significantly reduced at 70ºC. Gullapalli *et al.* (2009) showed that the strength of FRP-concrete pull-off samples can be increased if they are first heated to 40ºC, but that their strength is reduced if they carry sustained load while they are heated. The 'warm' temperature behavior of the adhesive joint is also important in the design of fire protection systems for FRP strengthening, which insulate the adhesive from the 'hot' temperatures in the fire. Fire tests on protected FRP strengthening have demonstrated the importance of the adhesive glass transition behavior (Blondtrock *et al.* 2001; Stratford *et al.* 2009), but it was not possible to directly observe the behavior of the bonded joint due to the presence of the fire protection and the difficulties of instrumentation in a fire.

Epoxy adhesive at elevated temperatures

The first step towards understanding the behavior of bonded FRP strengthening at warm temperatures is to characterise the behavior of the adhesive. Fig. 1 shows the glass transition behavior of a typical epoxy adhesive, plotted in terms of the change in the adhesive's elastic stiffness with temperature (where the stiffness has been normalised by its value at 20ºC). This response was obtained by dynamic mechanical analysis (DMA), which involves applying a sinusoidal displacement to a polymer specimen and measuring its load-displacement response with increasing temperature (ISO 6721, 2002). DMA gives a direct measure of mechanical properties that are relevant to the behavior of a bonded joint.

Fig. 1 plots the elastic or 'storage' modulus of the adhesive (for which the load and displacement are in phase), but DMA also measures the plastic or 'loss' modulus (load and deflection out of phase), and calculates the phase angle (δ) between the loss and storage moduli (Jaipuriar *et al*. 2010). The full glass transition data, however, is rarely reported, and only a single characteristic glass transition temperature (T_g) is usually recorded. For a DMA test, T_g occurs at the peak in the tanδ curve (ISO 6721, 2002), but it is important to note that there are a variety of methods for examining the glass transition, and that each can give a different value for T_g (Ludwig *et al*. 2008). It is thus important to state the test method and specific test parameters that have been used.

The adhesive characterised in Fig. 1 was used for the experimental work described later in this paper; its glass transition response is presented in this introductory section because it is typical of the two-part ambient cure epoxies that are sold specifically for FRP plate bonded strengthening. The DMA tests were conducted by the authors using a Triton Technology Tritec DS6010 machine in a double cantilever configuration (10×1×15mm clear span) at 1 Hz and 3ºC/min.

Fig. 1 shows that the glass transition phenomenon occurs over a range of temperatures from about 40ºC to around 70ºC. The ISO 6721 method gives T_g= 65ºC for the current adhesive, but at this temperature, the elastic stiffness of the adhesive is less than 10% of its 20ºC value. Far smaller reductions in stiffness are usually considered important in design; for example structural engineers often consider a 5% reduction in a mechanical property to be significant, which occurs for the stiffness of this adhesive when its temperature is increased from 20ºC to around 40ºC.

The reduction in adhesive stiffness through the glass transition is accompanied by a reduction in its strength, but an increase in its deformation capacity. Furthermore, the adhesive becomes viscoelastic at elevated temperatures, and consequently its complete constitutive response is non-linear and time-dependent (Ashby and Jones, 1986). Creep is known to affect the long-term performance of bonded FRP strengthening at ambient temperatures (Mazzotti and Savoia 2009), and consequently stress redistribution due to creep is even more significant at elevated temperatures. Gullapalli *et al.* (2009) demonstrated that the transfer length is affected by creep at warm temperatures by comparing concrete to FRP pull-off tests at 20ºC and 40ºC.

How do warm temperatures affect bonded FRP strengthening?

The implications of the adhesive's glass transition behavior for the overall performance of bonded FRP strengthening at warm temperatures are not obvious.

Bonded FRP strengthening relies upon the adhesive to transfer load between the strengthening plate and the beam, resulting in shear and normal ('peel') stresses within the adhesive, which are concentrated towards the end of the strengthening plate. The distribution of these bond stresses at ambient temperature has been researched in considerable detail, and a number of bond analysis models have been developed (e.g. Deng *et al*. 2004; Denton 2001; Smith and Teng 2001; Stratford and Cadei 2006). All use essentially the same analysis method: they assume linear-elastic materials, constant

stress through the adhesive thickness, and that failure occurs when the strength of the adhesive is reached at the end of the plate. Similar bond analyses are currently used in design (CIRIA 2004; CNR 2007; Schnerch *et al*. 2007).

The above bond analyses were developed for ambient temperatures. They include the effects of differential thermal expansion between the plate and beam, which can be larger than the bond stresses due to applied loads for a typical bridge strengthening scheme (Denton 2001). However, whilst the CIRIA (2004) design guide recommends that the stiffness of the adhesive should be reduced at temperatures approaching the glass transition temperature, the analyses do not examine how the changes in adhesive properties at warm temperatures affect the overall strength of the bonded strengthening. The reduced strength of the adhesive will be detrimental, but the adhesive's reduced stiffness and increased plastic deformation allow load transfer over a greater length of the adhesive joint and are hence beneficial in many situations. Consequently, the net effect of the glass transition is not clear.

Outline of the research presented in this paper

This paper investigates the performance of bonded FRP strengthening at warm temperatures through a combination of experimental and analytical work. The experimental investigation examined the behavior of the adhesive joint in CFRP-strengthened steel beams subjected to combined sustained load and transient increasing temperature.

The analytical work incorporates the adhesive glass transition response into a bond analysis for a FRP strengthened beam. A bond model that incorporates the full complexities of visco-elastic adhesive behavior is beyond the scope of the current paper; the aim is instead to use a simplified adhesive constitutive model to explore the significance of warm temperatures for bonded FRP strengthening, to highlight its importance in design, and to identify the need for further research.

TESTS ON CFRP STRENGTHENED STEEL BEAMS

Six steel I-beams were strengthened using CFRP plates and epoxy adhesive. Tests were conducted to establish the effects of sustained load and transient thermal exposure upon these beams. The beams were subjected to a sustained load that was greater than the capacity of the steel beam without strengthening. Their temperature was then increased until the strengthening system failed within the adhesive joint, resulting in failure of the strengthened beam. The performance of the adhesive joint was examined by measuring the slip of the strengthening plate relative to the beam.

Test method

The cross-section and material properties of the strengthened beams (as stated by the manufacturers) are shown in Fig. 2. The steel I-beams were standard 179mm deep sections with a yield strength of σ_u=355N/mm^2, and the cross-sectional area (A_b), major axis second moment of area (I_b), and Young's modulus (E_b) given in the figure. The beams were strengthened using a system manufactured specifically for structural applications, which combines pultruded CFRP plates with the epoxy adhesive

characterised in Fig. 1. The Young's modulus (E_a) and shear strength (τ_u) of the adhesive given in Fig. 2 are the manufacturer's stated values at 20ºC. Note the order of magnitude difference in coefficient of thermal expansion (α) between the CFRP plate and steel beam. The strengthening was applied to within 125mm of the beam supports (Fig. 3), using a nominal adhesive thickness of $t_a \approx 2$mm (which was verified after installation), and according to the manufacturer's instructions.

The beams were loaded in inverted 4-point bending over a 2m span, as shown in Fig. 3. A 5W/inch^2 (7.8kW/m^2) silicone rubber electrical heating pad, backed by a layer of insulation, was used to heat one end of the strengthening from above (figs 3 and 4). The heating pad was controlled by a thermocouple attached to the heated surface of the strengthened beam, 100mm from the end of the strengthening plate. Two further thermocouples were used to measure the temperature of the flange of the steel beam at the end of the plate (T_2) and 160mm from the end of the plate (T_1). These temperatures are assumed to have been equal to the local temperature of the bonding adhesive, due to the high thermal conductivity of the steel.

Table 1 summarises the tests conducted, together with headline results that will be discussed below. Three tests were conducted to determine the beams' load capacities at ambient temperature (18ºC to 20ºC). Tests 1 and 6 were used to find the ambient capacity of a strengthened beam, and Test 7 gave the ambient capacity of a steel beam without strengthening.

Beams 2 to 5 were tested under combined load and temperature. The beams were first loaded to above their unstrengthened ambient capacity at a rate of 10kN/min. This load was held constant while the temperature in the adhesive at T_2 was increased at a rate of 5.5ºC/min until failure occurred. Each of the ends of beams 4 and 5 were tested separately (tests 4a, 4b; 5a, 5b), giving a total of six heated tests.

Digital image analysis was used to determine the slip deformation that occurred between the strengthening plate and the beam. This technique allowed the variation in slip along the strengthening plate to be found, but did not require contact with the specimen (which could have affected the heat flow, and avoided the difficulties in attaching mechanical gauges to these tests). The side of the CFRP, adhesive and beam flange was painted with a high-contrast texture (figs. 4 and 5), and high-resolution digital images of the heated end of the plate were recorded at 10-second intervals. After the tests, the images were analysed using a bespoke digital image correlation algorithm (White *et al*. 2003). The slip displacement across the adhesive joint was determined by tracking the displacement of 100 patches of pixels in the plate relative to corresponding patches of pixels in the flange of the beam (shown schematically in Fig. 5). The measurement resolution for the camera's field of view used in these tests was around 0.002mm.

Experimental results

Table 1 summarises the key results from the tests, including the failure loads for the ambient tests, failure temperatures for the heated tests, and the modes of failure. Fig. 6 plots the failure temperatures against applied load.

The ambient tests determined the capacities of an unstrengthened (Test 7) and strengthened (Test 1) beam. Both tests failed by lateral-torsional buckling, and thus remained elastic up to failure. Test 6 was intended to confirm the ambient strengthened capacity, but failed prematurely due to air voids in the adhesive.

The heated tests were carried out for values of sustained load bounded by the ambient unstrengthened and strengthened tests (Fig. 6). Unfortunately no data were obtained from the test at 160kN. In all of the heated tests failure occurred when the strengthening plate debonded from the beam along the heated length, as shown in Fig. 4. The failure was adhesive, generally at the adhesive-steel interface, and inspection of the adhesive joint after testing showed that none of the heated specimens contained bond defects.

Debonding of the strengthening plate transferred the entire load in this part of the specimen into the unstrengthened beam, and caused a secondary, lateral-torsional buckling, failure (except for tests 4a and 5a, in which the load was removed immediately after the debonding event). This is consistent with the unstrengthened ambient test, but it should be noted that the heated beams all failed by debonding in the adhesive joint, and not by lateral torsional buckling. The image analysis software was used to check for the out-of-plane deformation that accompanies lateral-torsional buckling, and none was observed prior to debonding.

The failure temperatures plotted in Fig. 6 do not exhibit a discernible trend with the applied load. The temperature is plotted at both thermocouples, showing that the temperature at the plate end (T_2) was lower than the temperature within the plate (T_1) due to conduction into the unheated steel beam towards the supports (Fig. 3). This is a drawback of local heating using an electrical heating pad rather than uniform heating of the whole specimen; however, debonding failure initiated at the stress concentration at the end of the plate, and thus T_2 is more representative of the failure temperature.

Observed slip displacements

An example of the output from the digital image correlation analysis is shown in Fig. 7 for Test 5B, and similar results were obtained from the other tests. This figure plots the slip displacement along the adhesive joint over a 60mm length from the end of the strengthening plate, and for increasing temperature. The slip displacements were small up to around 40°C, after which the slip increased until failure occurred at 64°C and a slip of 0.22mm. At temperatures up to around 45°C the slip increased towards the centre of the beam, which is believed to be due to differential thermal expansion resulting from the temperature gradient from T_1 to T_2 noted above. Above 45ºC, there was little variation in the magnitude of the slip along the observed length of the adhesive joint, indicating that slip also occurred outside the field of view of the camera towards the centre of the beam.

Close to failure the maximum slip for all specimens was at the end of the strengthening plate, and so far as it was possible to tell, failure initiated at this position. Fig. 8 plots the plate-end slip displacements against temperature for all of the tests. In all cases significant slips occur from about

40°C, and these slips grew until failure occurred at approximately 65°C (the ISO 6721 glass transition temperature). The maximum recorded slips before failure were in the range 0.16 to 0.23mm, but it should be noted that the actual failure slip will have been higher, because the last image could have been taken up to 10 seconds prior to failure.

The digital image correlation analysis was also used to observe peel deformations, but it was not possible to detect any meaningful peel deformations prior to debonding failure (i.e.: any deformation that did occur was smaller than the measurement resolution of about 0.002mm).

ANALYSIS OF CFRP STRENGTHENED BEAMS AT WARM TEMPERATURES

As noted in the Introduction, the effect of warm temperatures upon bonded FRP strengthening is not currently considered in design, except for a reduction in the elastic adhesive stiffness in the CIRIA (2004) design guide. In this section, the effects of the adhesive glass transition are incorporated into a new bond model and this analysis is used to examine the plate slip deformation and debonding failure observed during the experiments.

The non-linear and time-dependent behavior of the adhesive means that a complete bond analysis is complex, and beyond the scope of this paper. The approach taken here is to use a simplified model for the adhesive glass transition that gives further insights into the experimental results, improves upon the purely elastic method currently used in design, and raises awareness of potential warm temperature effects that require additional research.

A bond model for warm temperatures

The bond analysis is described in detail in the appendix to this paper. It is based upon the models currently used to predict adhesive stresses at ambient temperatures (Deng *et al.* 2004; Denton 2001; Smith and Teng 2001; Stratford and Cadei 2006); however, the new bond model uses an adhesive constitutive model that takes into account the variation in properties with temperature. The effects of both applied load and differential thermal expansion between the plate and flange of the beam are included, but note that the model is only concerned with shear across the adhesive joint (as observed experimentally); it does not consider peel.

The adhesive is modelled using the idealised elasto-plastic constitutive model shown in Fig. 9. The shear modulus (G_a) and shear strength (τ_u) of the adhesive reduce with temperature. The reduction in shear strength with temperature has not been characterised, and will not exactly follow the reduction in shear modulus (Ashby and Jones, 2006); however, both are determined from the glass transition data in Fig. 1. The shear modulus and shear strength at a particular temperature are found by multiplying the value at 20ºC by the normalised stiffness from Fig. 1. At low temperatures the adhesive is brittle, but at elevated temperatures the adhesive undergoes plastic deformation before rupture, modelled as a horizontal plastic plateau. The adhesive's strain capacity at rupture increases with temperature; however, adhesive rupture is not modelled and it will be seen below that failure is not sensitive to the strain capacity of the adhesive.

Analytical results

The warm temperature bond model was used to examine the behavior of the test beams. The model used the specimen geometry and properties shown in figs. 2 and 3. The adhesive shear strength and stiffness at 20ºC were τ_u = 17MPa and G_a = 3.8GPa (based upon the manufacturer's values given in Fig. 2 and a Poisson's ratio of 0.3), and these were reduced with temperature according to the glass transition curve in Fig. 1. No experimental results other than the DMA data were used as inputs to the analysis.

Plate end slip with temperature for different applied loads

Fig. 10 plots the plate end slip predicted by the bond analysis for different applied loads.

The 150kN and 180kN responses represent the sustained loads applied during the tests. For these loads, significant slip deformation occurs from around 40°C, and increases with temperature. The slip increases rapidly up to a temperature of 64.0ºC for 180kN, or 65.6ºC for 150kN (off the top of Fig. 10), when failure occurs. It will be shown below that this failure temperature occurs when the whole length of the adhesive joint is plastic. This results in debonding of the strengthening from the beam, followed by failure of the steel beam (which is unable to carry the applied load). The rapid increase in plate end slip with temperature prior to failure means that the failure temperature is not sensitive to the strain capacity of the adhesive, nor the adhesive failure criteria between the adhesive and the substrates, which are not included in the analysis. However, the failure temperature could be affected by loading and heating rate due to viscoelastic effects that are outside the scope of the current study.

The 150kN and 180kN curves are shown as a grey band in Fig. 8 to allow direct comparison with the experimental results. The analytical response follows the same trend as the experiments: the slip starts to increase from about 40ºC, and increases rapidly towards a failure temperature of around 65ºC. The analysis predicts little variation in the failure temperature for the range of loads applied during the tests, as observed during the experiments (Fig. 6). Failure in both the tests and the analysis occurs by debonding of the FRP plate, although the analysis does not predict the slip at which the adhesive strain capacity is reached. Whilst the failure temperature and mechanism are in reasonable agreement, the slip is under predicted at lower temperatures. This is because the analysis assumes uniform temperature along the beam, and does not include the variation in temperature that was present along the beam during the tests (Fig. 6).

A real strengthening project would not be designed to carry service loads greater than the unstrengthened capacity of the beam, which was 140kN in the present case. For reduced loads (the 100kN, 50kN curves in Fig. 10), the analysis predicts rapid increases in slip with temperature that would result in debonding of the strengthening, but at higher temperatures. Slip occurs along the adhesive joint even if the beam is unloaded, due to differential thermal expansion between the beam and strengthening plate. Viscoelastic creep would increase the slip magnitude under sustained serviceability loads.

Distributions of slip and shear stress along the adhesive joint

The bond analysis can be used to examine load transfer between the strengthening plate and the beam in greater detail than was possible during the experiments.

Fig. 11 plots the slip distribution over a 60mm length of the adhesive joint for increasing temperatures. This figure is for 180kN applied load, and can thus be directly compared to the experimentally observed slip distribution shown in Fig. 7. The slip distribution in Fig. 11 increases towards the end of the strengthening plate (x=0), unlike the observed slips at low temperatures, which increased towards the centre of the beam. However, it has already been noted that this was due to the temperature gradient along the beam, which is not included in the analysis. At higher temperatures, the variation in slip is small compared to the magnitude of the slip in both the experimental and analytical results, indicating that all of the adhesive along the 60mm observed length is plastic.

Fig. 12 and 13 plot the slip and shear stress distribution along half of the beam length for an applied load of 180kN, rather than only the 60mm observed length. At 20ºC, the adhesive is elastic, and the shear stress and slip are concentrated at the end of the plate. Away from the plate end, the shear stress distribution is as predicted by simple beam theory, with a jump in shear stress at the loading point (x = 475mm). As the temperature is increased to 40ºC, differential thermal expansion causes an increase in the plate end slip and shear stress. Above 40ºC, the adhesive loses strength and becomes plastic. A plastic zone forms at the plate end, visible as a plateau in the shear stress distribution at 50ºC, and this plastic zone spreads along the adhesive joint as the temperature is increased, accompanied by rapidly increasing slip. Failure occurs when the plastic zone reaches the centre of the beam at slightly over 64ºC. (The maximum slip at 60ºC and 64ºC is off the top of Fig. 12, but can be seen in Fig. 11).

The significance of the different components of adhesive joint behavior

Fig. 14 compares the importance of different components of adhesive joint behavior at elevated temperature, for a 180kN applied load. The figure plots the plate end slip for:

(a) An analysis for 180kN applied load that includes differential thermal expansion and adhesive properties that change with temperature.

(b) An unloaded beam, in which the bond stresses are due to differential thermal expansion alone.

(c) A loaded beam, with adhesive properties that change with temperature, but with no differential thermal expansion.

(d) An elastic analysis, in which the shear stiffness of the adhesive varies with temperature, but the adhesive strength is not changed.

(e) An elastic analysis, in which the variation of adhesive properties with temperature is ignored.

Fig. 14 shows that all these effects need to be modelled to predict failure at warm temperatures.

Unsurprisingly, analysis based upon a purely elastic analysis (case (e)) does not predict the substantial slips that occur at elevated temperature. The CIRIA (2004) design guide recommends that the stiffness of the adhesive should be reduced at temperatures approaching the glass transition temperature; however, case (d) shows that even if the actual reduction in adhesive shear stiffness is known, an elastic analysis massively under-predicts the slips that occur, and hence does not predict the debonding failure that can occur.

Fig. 14 demonstrates that differential thermal expansion between the plate and the beam contributes to the slip deformation that occurs prior to failure. Note that the analysis only considers differential thermal expansion between the plate and the strengthened flange of the beam, and assumes a linear thermal gradient through the depth of the beam. Additional restrained thermal stresses would have resulted during the tests due to the non-linear thermal gradient through a beam's depth, which would have reduced the difference between case (a) and case (b). In the case considered here, however, the majority of the slip is due to the applied load, rather than differential thermal expansion.

CONCLUSIONS

The test results presented in this paper demonstrate that warm temperatures can significantly reduce the strength of an FRP-plated steel beam, and that large slip deformation occurs across the adhesive joint prior to failure. The glass transition process of a typical ambient cure epoxy adhesive is characterised by a single glass transition temperature of 65ºC according to ISO 6721 (2002); however, the adhesive loses both stiffness and strength over a range of temperatures. During the beam tests, significant slips were observed above 40ºC, and these slips increased with temperature until a debonding failure occurred at approximately the glass transition temperature of the adhesive. It should be noted, however, that Test 5A failed before the glass transition temperature was reached, at 60ºC.

Current design guidance recommends that the glass transition temperature of the adhesive must be at least 15ºC above the operating temperature (ACI 2008), suggesting a maximum operating temperature of 50ºC for the adhesive used in these tests. 0.13mm slip (or 6.5% shear strain) was recorded at 50ºC during tests 4B and 5A (Fig. 11). This slip may be acceptable, but it is not predicted or considered by the current elastic design methods for bonded FRP strengthening.

The analysis presented in this paper incorporates a simple elasto-plastic model of the adhesive glass transition into a bond analysis of the strengthened beam. By modeling the combined effects of adhesive strength and stiffness reduction through the glass transition and differential thermal expansion between the strengthening plate and beam, the analysis suggests that failure is due to a rapid increase in slip as

the plastic adhesive zone spreads along the whole length of the beam, and consequently the failure temperature is not sensitive to the strain capacity of the adhesive joint.

The tests were carried out under sustained load and transient increasing temperature. For the beam geometry, properties, and heating rate considered, both the tests and analysis suggest that the failure temperature is insensitive to the applied load, if the load is greater than the capacity of the unstrengthened beam.

This paper does not examine the effects of time-dependent constitutive behavior of the adhesive at warm temperatures: the bond analysis is elasto-plastic, and the tests were conducted using a single, transient, heating rate. Creep of the adhesive is known to be important in long-term performance tests at 20ºC (Mazzotti and Savaoia 2009), and will be similarly important for bonded FRP subjected to sustained warm temperatures. Despite this, the tests and analysis presented in this paper, demonstrate the importance of warm temperatures upon bonded FRP strengthening and are an improvement upon previous design practice.

ACKNOWLEDGEMENTS

The experiments were undertaken by Cameron Gillespie and Martin Moran during their undergraduate theses, and the School of Engineering at the University of Edinburgh is thanked for its support of these projects. Dr Andy Take of Queen's University, Canada, is thanked for allowing access to the GeoPIV digital image correlation software. The Scottish Funding Council is thanked for its support of the Joint Research Institute for Civil and Environmental Engineering, part of the Edinburgh Research Partnership in Engineering and Mathematics (ERPem). Bisby gratefully acknowledges the support of the Ove Arup Foundation and the Royal Academy of Engineering.

APPENDIX: ANALYSIS OF ADHESIVE BOND AT WARM TEMPERATURES

This appendix describes a bond analysis that predicts the shear strain (γ_a) and shear stress (τ_a) distributions between a strengthening plate and a beam and allows the effect of temperature-dependent adhesive properties to be examined. The problem's parameters are defined in Fig. 15:

- The beam is defined by its cross-sectional area (A_b), second moment of area (I_b), the position of its neutral axis (y_b), Young's modulus (E_b), and coefficient of thermal expansion (α_b). It carries a moment and axial force of M_b and N_b.

- The strengthening plate is defined by similar parameters (A_s, I_s, y_s, E_s, α_s, M_s, N_s).

- The adhesive is defined by its thickness (t_a) and breadth (b_a). The adhesive is modelled using the idealised elasto-plastic constitutive relationship shown in Fig. 9, using glass transition data (such as that in Fig. 1) to modify the ambient properties.

The strengthening plate and top flange of the beam are subjected to a temperature change ΔT. The remainder of the beam is assumed to have a linear thermal gradient (or a uniform temperature change) through its depth, otherwise additional restrained thermal expansion stress will develop within the beam. The bending moment distribution along the beam is M, which for the four-point bending case considered in this paper with loads $W/2$ applied at a distance b from the plate end (Fig. 3) is:

$$M = \frac{W}{2}\left\{ \left(x + a\right) - \left\langle x - b \right\rangle \right\} \tag{1}$$

x is the position along the beam from the plate end, which is a distance a from the support (see Fig. 16). $\langle x\text{-}b \rangle$ is a Macaulay bracket.

Derivation of the governing equation for adhesive shear

Shear compatibility across the adhesive joint requires that the strain in the strengthening (ε_s) and beam (ε_b) are related to the adhesive shear strain (γ_a) by:

$$t_a \frac{d\gamma_a}{dx} = \varepsilon_{sa} - \varepsilon_{ba} \tag{2}$$

These strains are the result of plane-section deformation of the strengthening plate and beam due to bending, axial force, and thermal expansion:

$$\varepsilon_{sa} = \frac{N_s}{E_s A_s} - \frac{M_s y_s}{E_s I_s} + \alpha_s \Delta T \qquad \text{and} \qquad \varepsilon_{ba} = \frac{N_b}{E_b A_b} - \frac{M_b y_b}{E_b I_b} + \alpha_b \Delta T \tag{3}$$

Equilibrium requires that the axial force and bending moment in the beam (Fig. 15) can be written in terms of the strengthening stress resultants and the net bending moment:

$$N_b = -N_s \qquad \text{and} \qquad M_b = M - M_s - N_s z \tag{4}$$

To simplify the solution, the moment carried in the relatively flexible strengthening plate can be assumed negligible compared to the moment carried by the beam, i.e.: M_s=0 (Deng *et al*. 2004). Combining eqns (2), (3), and (4) thus gives:

$$t_a \frac{d\gamma_a}{dx} = \frac{k}{b_a} N_s - \frac{M y_b}{E_b I_b} + \left(\alpha_s - \alpha_b\right)\Delta T \tag{5}$$

where

$$k = b_a \left[\frac{1}{E_s A_s} + \frac{1}{E_b A_b} + \frac{z y_b}{E_b I_b} \right] \tag{6}$$

Differentiating Eqn. (5) gives:

$$t_a \frac{d^2\gamma_a}{dx^2} = \frac{k}{b_a}\frac{dN_s}{dx} - \frac{y_b}{E_b I_b}\frac{dM}{dx} \tag{7}$$

Axial equilibrium of a short length of the plate (Fig. 16) gives the adhesive shear stress in terms of the rate of change in plate force:

$$\tau_a = \frac{1}{b_a}\frac{dN_s}{dx} \tag{8}$$

Substituting Eqn (8) into Eqn (7) yields the governing equation for shear in the adhesive joint. This relates the shear strain and stress, but does not include the adhesive constitutive relationship (Fig. 9):

$$t_a \frac{d^2\gamma_a}{dx^2} = k\tau_a - \frac{y_b}{E_b I_b}\frac{dM}{dx} \tag{9}$$

General solutions where the adhesive is elastic or plastic

If the adhesive is elastic, $\tau_a = G\gamma_a$ (Fig. 9), and the general solution to Eqn (9) is:

$$\gamma_a = C_1 e^{-\lambda x} + C_2 e^{+\lambda x} + \frac{W y_b}{2kG_a E_b I_b}\left\{1 - \langle x-b\rangle^0\right\} \tag{10}$$

where Eqn. (1) has been used to substitute the applied load for the net moment, and

$$\lambda = \sqrt{\frac{kG_a}{t_a}} \tag{11}$$

If the adhesive is plastic, $\tau_a = \tau_u$ (Fig. 9), and the general solution to Eqn (9) is:

$$\gamma_a = \frac{k\tau_u}{2t_a}x^2 - \frac{W y_b}{4E_b I_b t_a}\left\{x^2 - \langle x-b\rangle^2\right\} + C_3 x + C_4 \tag{12}$$

Boundary conditions

The applied loading is symmetrical, and the heated region is remote from the centre of the beam, hence the adhesive shear strain is assumed to be zero at the centre of the beam. (This assumption would not be valid if shorter beams were heated at one end, or if the heated area was longer relative to the beam length). At the end of the strengthening the plate force must be zero. Substituting N_s=0 into Eqn (5) gives the plate end boundary condition in terms of the shear strain:

$$\left[\frac{d\gamma_a}{dx}\right]_0 = \frac{1}{t_a}(\alpha_s - \alpha_b)\Delta T - \frac{Way_b}{2t_a E_b I_b} \tag{13}$$

The adhesive can either be entirely elastic ($\gamma_a<\gamma_u$ along the whole of the plate, as shown on the left of Fig. 16), or will be elasto-plastic with a plastic zone towards the plate end (as shown on the right of Fig. 16). For the purely elastic case, applying the boundary conditions to the general solution (Eqn 10) gives:

$$C_1 = \frac{-1}{\lambda\left(1+e^{-\lambda L}\right)}\left[\frac{d\gamma_a}{dx}\right]_0 \tag{14}$$

$$C_2 = -C_1 e^{-\lambda L} \tag{15}$$

For the elasto-plastic case, the shear strain must be continuous at the transition between the elastic and plastic zones (Fig. 16), in addition to the above two boundary conditions. The position of the transition ($x=p$) needs to be determined. Applying the boundary conditions in the elastic zone (Eqn 10) gives:

$$C_1 = \frac{1}{e^{-\lambda p} - e^{\lambda(p-L)}}\left(\gamma_u - \frac{Wy_b}{2kG_a E_b I_b}\left\{1 - \langle p-b\rangle^0\right\}\right) \tag{16}$$

$$C_2 = -C_1 e^{-\lambda L} \tag{17}$$

Applying the boundary conditions in the plastic zone (Eqn 12):

$$C_3 = \left[\frac{d\gamma_a}{dx}\right]_0 \tag{18}$$

$$C_4 = \gamma_u - \frac{k\tau_u}{2t_a}p^2 + \frac{Wy_b}{4E_b I_b t_a}\left\{p^2 - \langle p-b\rangle^2\right\} - C_3 p \tag{19}$$

The length of the plastic zone (p) is found from the condition that the plate force must be continuous at the elastic-plastic transition, which requires continuity of $d\gamma_a/dx$, from Eqn (5). Applying continuity in $d\gamma_a/dx$ at $x=p$ to the elastic and plastic general solutions (eqns 10 and 12) gives an equation in which p is the sole unknown:

$$\lambda\frac{1+e^{\lambda(2p-L)}}{1-e^{\lambda(2p-L)}}\left(\gamma_u - \frac{Wy_b}{2kG_a E_b I_b}\left\{1-\langle p-b\rangle^0\right\}\right) = \frac{Wy_b}{2E_b I_b t_a}\left\{p - \langle p-b\rangle\right\} - \frac{k\tau_u}{t_a}p - \left[\frac{d\gamma_a}{dx}\right]_0 \tag{20}$$

This equation must be solved numerically, but once it has been used to determine the length of the plastic zone, the elasto-plastic solution is fully defined.

Outputs from the bond analysis

The bond analysis determines the shear strain (γ_a) variation along the adhesive joint, which is given by Eqn (10) in the elastic region ($\gamma_a<\gamma_u$) or Eqn (12) in the plastic region ($\gamma_a>\gamma_u$). In addition:

- The shear strain can be interpreted as a slip deformation, $s = t_a \gamma_a$ (21)

- The shear stress distribution (τ_a) can be found from the shear strain using the constitutive relationship in Fig. 9.

- The plate force (N_s) can be found from Eqn. (6), using $d\gamma_a/dx$ from Eqn (10) or Eqn (12).

REFERENCES

ACI. (2008). "Guide for the Design and Construction of Externally Bonded FRP Systems for Strengthening Concrete Structures." *American Concrete Institute Report ACI 440.2R-08*, Farmington Hills, MI.

Ashby M.F., Jones D.R.H., (1986). "Engineering Materials 2." *Pergamon Press*, Oxford.

Blondtrock H., Taerwe L., Vandevelde P., (2001). "Fire Testing of Concrete Slabs Strengthened with Fibre Composite Laminates." *Proceedings of FRPRCS-5*, Thomas Telford, London.

CIRIA (2004). "Strengthening metallic structures using externally bonded fibre-reinforced polymers." *Report C595*, London, UK.

CNR (2007). "Guidelines for the Design and Construction of Externally Bonded FRP Systems for Strengthening Existing Structures. Metallic Structures." *Italian National Research Council Report CNR-DT 202/2005*, Rome.

Concrete Society (2004). "Design guidance for strengthening concrete structures using fibre composite materials." *Technical Report 55*, 2nd edition, Camberley, UK.

Deng J., Lee M.M.K. and Moy S.S.J. (2004). "Stress analysis of steel beams reinforced with a bonded CFRP plate." *Composite Structures*, 65, 205–215.

Denton S.R. (2001). "Analysis of stresses developed in FRP plated beams due to thermal effects." *1st International Conference on FRP Composite in Civil Engineering*, Hong Kong, 527–536.

Gullapalli A., Lee J.H., Lopez M.M., Bakis C.E. (2009). "Sustained loading and temperature response of fiber-reinforced polymer-concrete bond." *Transportation Research Record: Journal of the Transportation Research Board*, 2131, 155-162.

Highways Agency. (2001). "BD37/01: Loads for highways bridges." *Design Manual for Roads and Bridges*, The Stationary Office Ltd., London, UK.

IS0 6721-1. (2002). "Plastics. Determination of dynamic mechanical properties. General principles." BSI, London, UK.

Jaipuriar A., Flood J.P., Bakis C.E., Lopez M.M., and He X. (2010). "Glassy-Rubbery Transition Behavior of Epoxy Resins used in FRP Structural Strengthening Systems", *5th International Conference on FRP Composites in Civil Engineering*, Beijing.

Klamer E.L., Hordijk D.A., Hermes M.C.J. (2008). "The influence of temperature on RC beams strengthened with externally bonded CFRP reinforcement." *Heron.* 53, 3, 157-186

Kodur, V.K.R., Bisby, L.A. and Green, M.F. (2007). "Preliminary guidance for the design of FRP-strengthened concrete members exposed to fire." *Journal of Fire Protection Engineering*, 17(5), 5-26

Ludwig C., Knippers J., Hugi E., and Ghazi Wakili K. (2008). "Damage of flexural loaded composite beams subjected to fire." *4th International Conference on FRP Composites in Civil Engineering*, Zurich, 527–536.

Mazzotti C., Savoia M. (2009), "Stress redistribution along the interface between concrete and FRP subject to long-term loading". *Advances in Structural Engineering*, 12(5), 561-661.

Porter M.L., Harries K., (2007). "Future Directions for Research in FRP Composites in Concrete Construction", *ASCE Journal of Composites for Construction*, 11(3), 252-257.

Schnerch D., Dawood M., Rizkalla S. (2007). "Design guidelines for the use of HM strips: Strengthening of steel concrete composite bridges with high modulus carbon fibre reinforced polymer (CFRP) strips." *Technical Report No. IS-06-02*, Constructed Facilities Laboratory, North Carolina State University.

Smith S.T. and Teng J.G. (2001). “Interfacial stresses in plated beams.” *Engineering Structures*, 23, 857–871.

Stratford T. and Cadei J. (2006). “Elastic analysis of adhesion stresses for the design of a strengthening plate bonded to a beam.” *Construction and Building Materials*, 20, 34-45.

Stratford T.J., Gillie M., Chen J.F. and Usmani A.S. (2009). “Bonded Fibre Reinforced Polymer Strengthening in a Real Fire.” *Advances in Structural Engineering*, 12(6), 867-878.

White D.J., Take W.A. and Bolton M.D. (2003). “Soil deformation measurement using particle image velocimetry (PIV) and photogrammetry.” *Geotechnique*, 53(7), 619-631

Table 1 Details of the experimental program and headline results.

	Test ID	Load (kN)	Temperature T_2 (ºC)	Comment
Ambient tests	1	190.0	Ambient	Capacity of a strengthened beam (l.t. buckling).
	6	(155.6)	Ambient	Premature failure due to poor bonding.
	7	140.4	Ambient	Capacity of an unstrengthened beam (l.t. buckling).
Heated tests	2	150	65	Plate debonding failure.
	3	160	Not available	Data acquisition error.
	4a	170	74	Plate debonding failure.
	4b	170	74	Plate debonding failure.
	5a	180	60	Plate debonding failure.
	5b	180	64	Plate debonding failure.

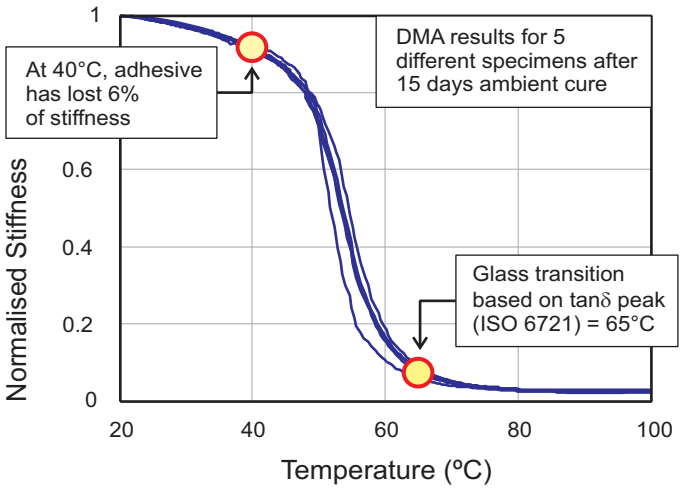

Fig. 1 - Measured loss in elastic stiffness of the epoxy bonding adhesive through the glass transition.

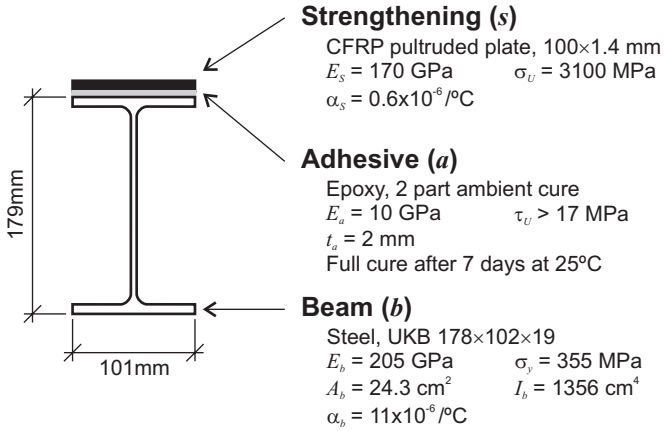

Fig. 2 - Cross-sectional dimensions and material properties of the strengthened beams (manufacturers' data sheet values).

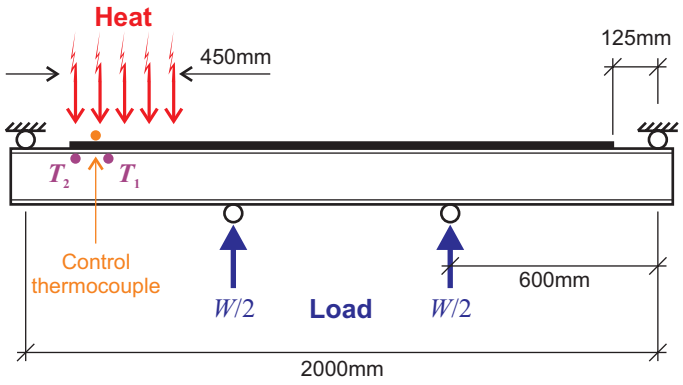

Fig. 3 - Schematic experimental set up, showing the loading and heating arrangements.

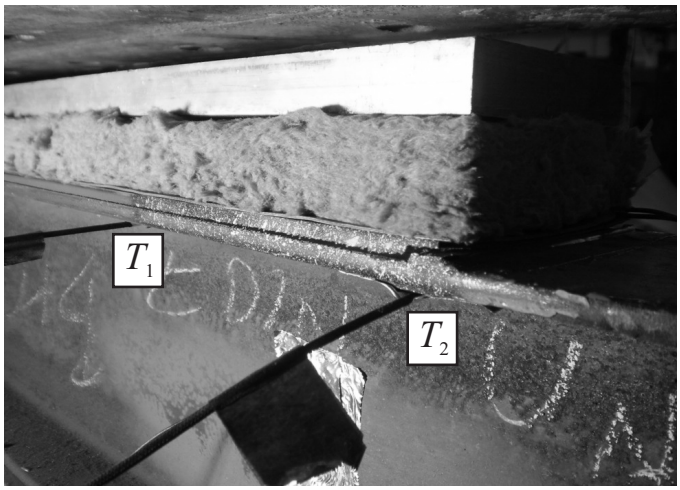

Fig. 4 - The heated end of a strengthening plate following debonding failure, showing the heating pad and thermocouples.

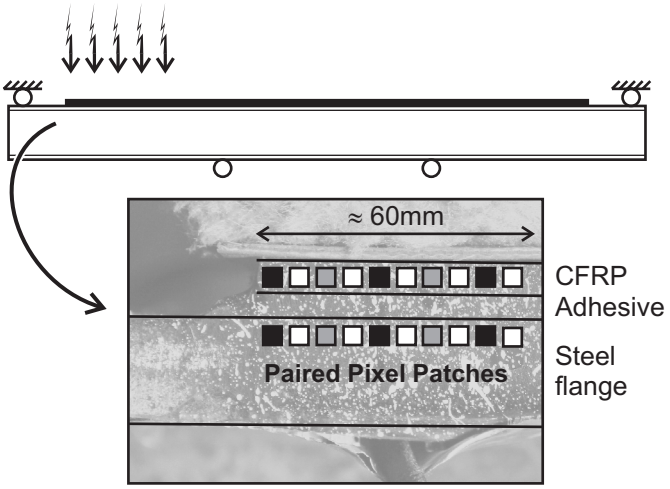

Fig. 5 - The measurement of slip displacements across the adhesive joint by digital image analysis.

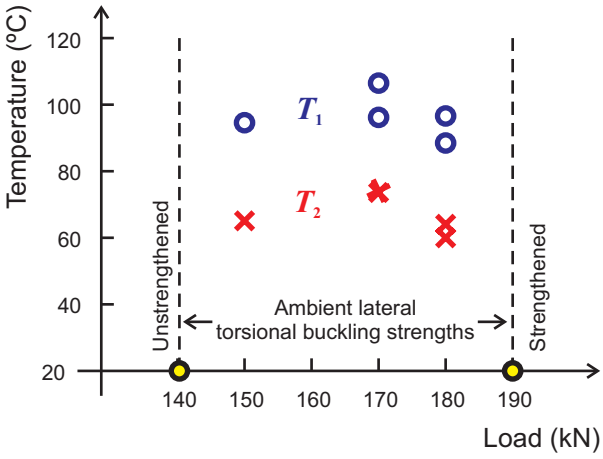

Fig. 6 - The failure temperatures for strengthened beams carrying different loads.

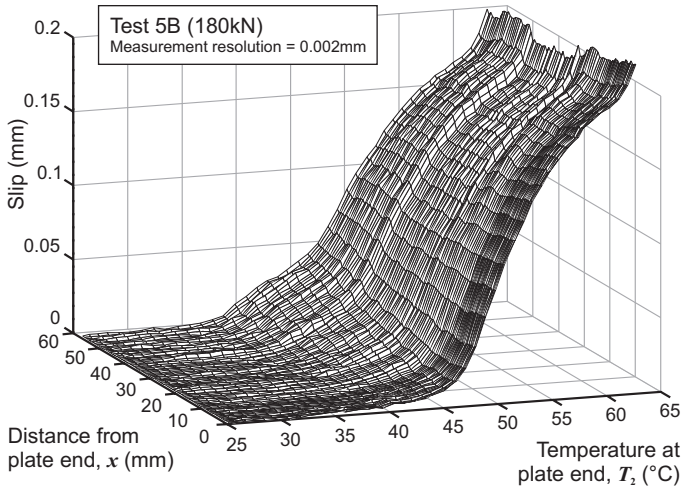

Fig. 7 - The observed variation in slip distribution along the plate with temperature, for Test 5B.

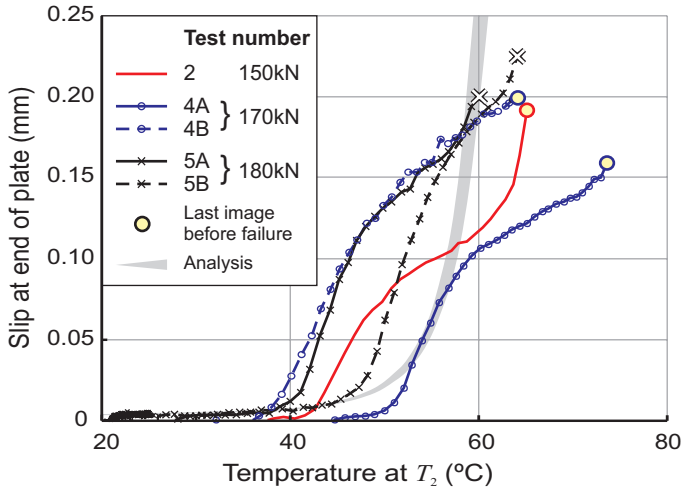

Fig. 8 - The observed variation in plate end slip with temperature.

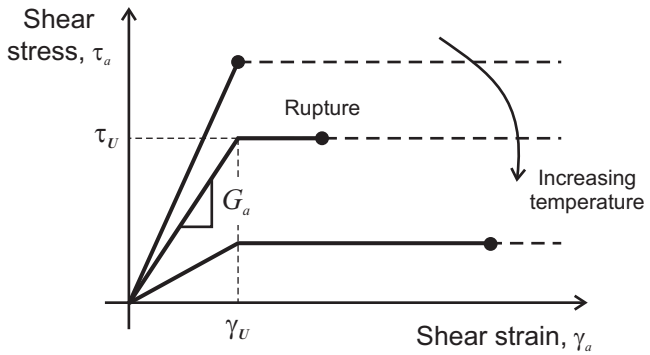

Fig. 9 - The elasto-plastic adhesive constitutive model used in the bond analysis.

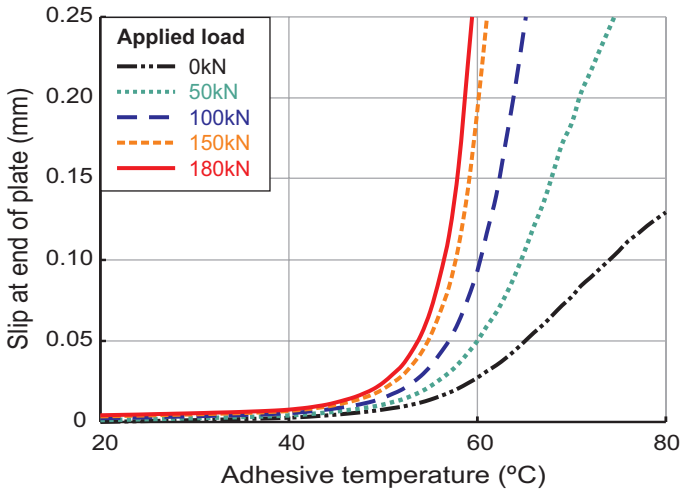

Fig. 10 - Plate end slip variation with temperature predicted by the bond analysis.

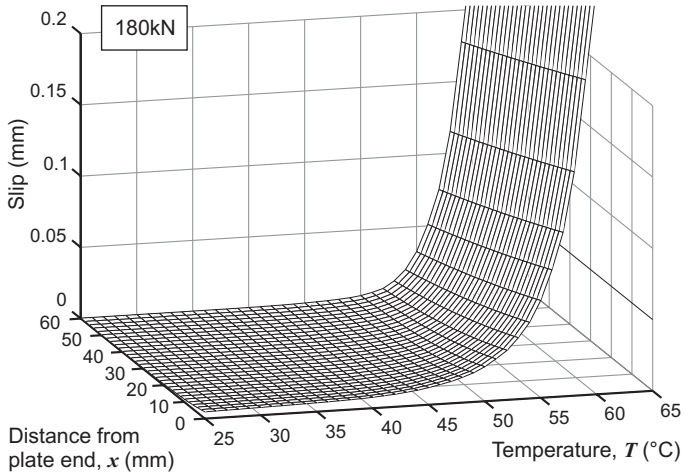

Fig. 11 - The variation in slip distribution along the plate with temperature, for a load of 180kN.

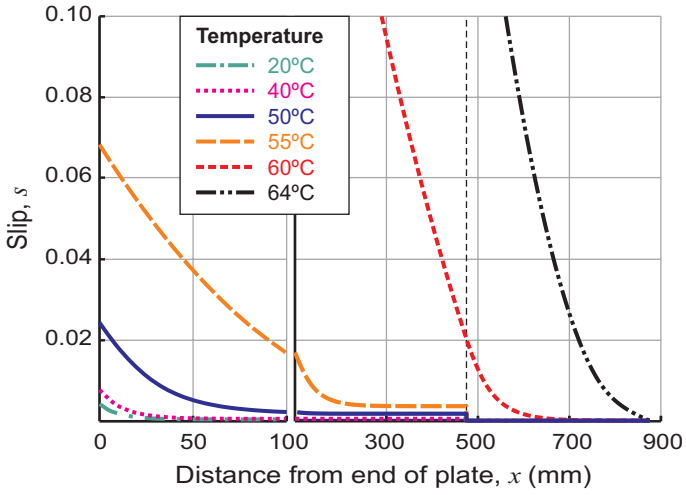

Fig. 12 - The slip distribution along the adhesive joint for a load of 180kN at various temperatures.

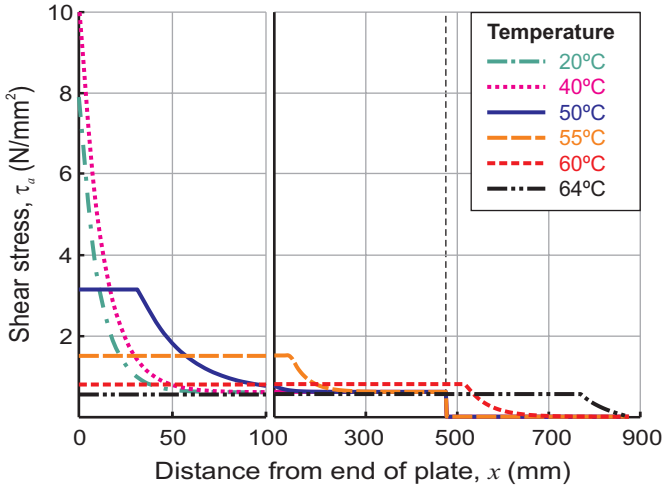

Fig. 13 - The shear stress distribution along the adhesive joint for 180kN load at various temperatures.

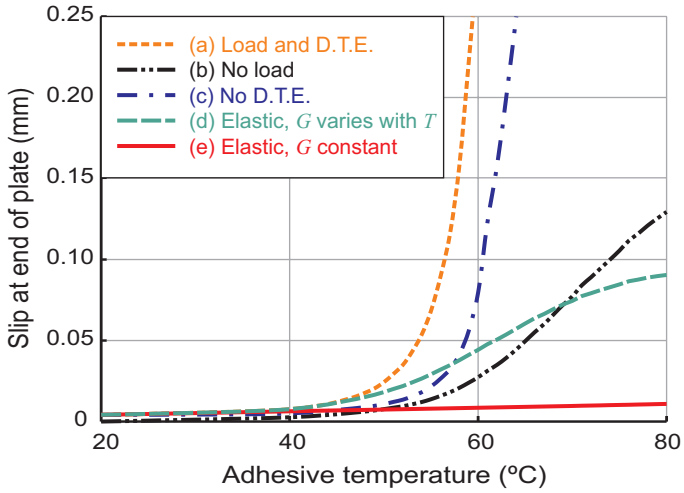

Fig. 14 - Plate end slip predictions for a load of 180kN, showing the effects of applied load, differential thermal expansion, and adhesive properties.

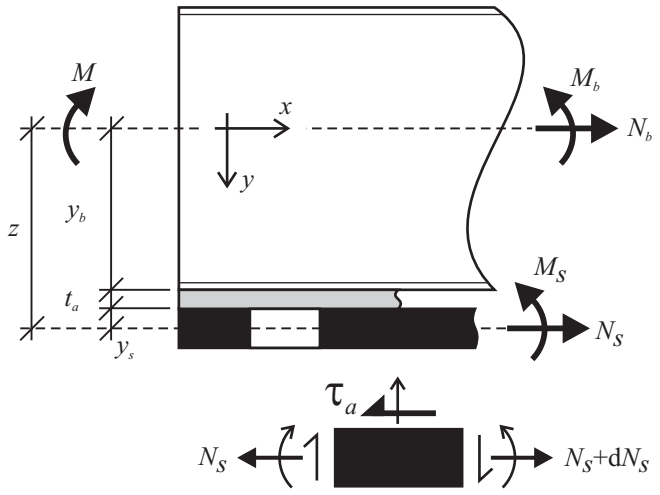

Fig. 15 - Definitions of beam, adhesive and strengthening plate geometry and stress resultants for the bond analysis.

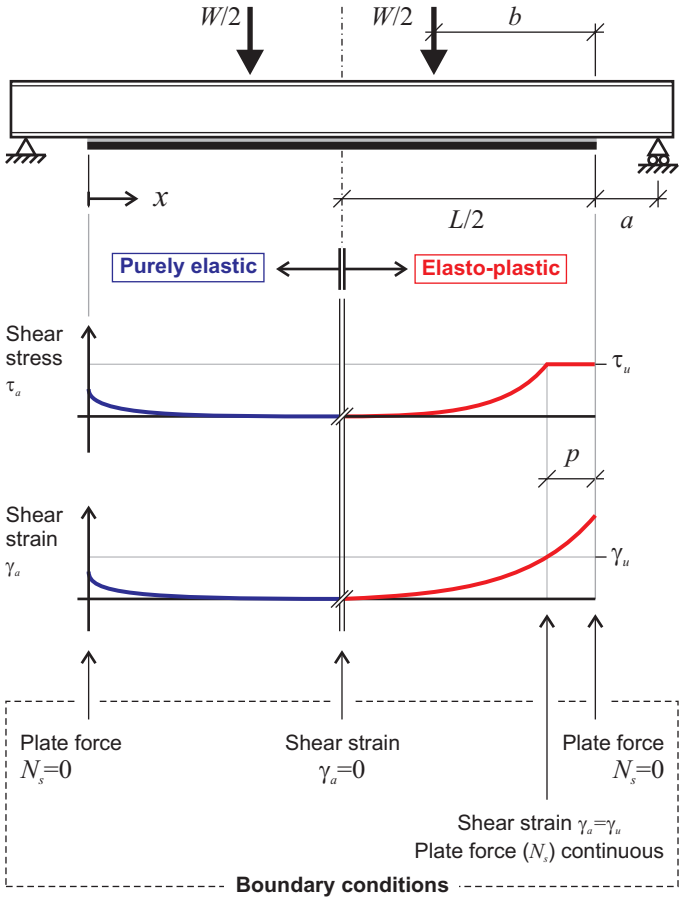

Fig. 16 - Definitions of the beam geometry, applied load and boundary conditions for the bond analysis.